12. A. C. Griffin and S. J. Havens, *J. Polym. Sci. Polym. Phys. Ed.*, **19**, 956 (1981).
13. E. Fischer and H. O. L. Fischer, *Ber.*, **46**, 1138 (1913).
14. E. Fischer and K. Freudenberg, *Ann.*, **372**, 32 (1910).
15. J. H. Wilkinson, W. E. Sprott and N. F. MacLagan, *Biochem. J.*, **54**, 16 (1953).
16. P. L. Barny, G. Ravaux, J. C. DuBois and J. P. Parneix, *Mol. Cryst. Liq. Cryst.*, **127**, 413 (1985).
17. A. C. Griffin, R. B. Britt, N. W. Buckley, R. F. Fisher, J. S. Havens and D. W. Goodman in *'Liquid Crystals and Ordered Fluids*, Vol. 3', ed. by J. F. Johnson and R. S. Porter, Plenum Press, New York, 1978, pp. 61-73.
18. N. A. Vaz, S. L. Arora, J. W. Doane and A. DeVries, *Mol. Cryst. Liq. Cryst.*, **128**, 23 (1985).
19. I. Tanaka and H. Hori, *'Synthetic Method and Application of Liquid Crystals* (in Japanese), Sai-Wai Publishers, Tokyo, 1979, p. 112-112.
20. G. W. Gray and P. A. Winsor, Ed., *'Liquid Crystals & Plastic Crystals'*, Vol. 1, Ellis Horwood Publisher, London, 1974, pp. 138-142.
21. Reference 20, p. 108.

Oxygen Interstitial Defects and Ion Hopping Conduction of X ThO_2 + (1 − X) Gd_2O_3 Solid Solutions: $0.08 \leq X \leq 0.12$

Sung Ho Park†, Yoo Young Kim, and Keu Hong Kim*

Department of Chemistry, Yonsei University, Seoul 120-749
†Department of Chemistry, Chonju University, Chonju 560-759. *Received March 23, 1990*

Gd_2O_3-ThO_2 solid solutions containing 8, 10 and 12 mol % ThO_2 were synthesized with spectroscopically pure Gd_2O_3 and ThO_2 polycrystalline powders. X-ray diffraction revealed that all synthesized specimens have the modified fluorite structure, and the lattice parameter of Gd_2O_3 is nearly unchanged with increasing ThO_2 mol %. Both *ac* and *dc* conductivities were measured in the temperature range 500-1100 °C under Po_2's from 10^{-6} to 10^{-1} atm. The *dc* conductivities are nearly independent of Po_2, and agree with the *ac* values. This implies that the solid solutions are ionic conductors. The conductivity increases with increasing ThO_2 mol % with an average activation energy of 1.23 eV. An oxygen interstitial defect and ionic hopping conduction are suggested.

Introduction

Gd_2O_3 is one of the lanthanide oxides and is known to have cubic C-type structure with lattice constant 10.813 Å at temperatures up to 1200 °C. There are 24 Gd^{3+} ions on sites with two-fold rotational symmetry (C_2), 8 Gd^{3+} ions on sites with three-fold rotatory inversion symmetry (C_3), the 48 rotatory O^{2-} ions at general positions, and 16 interstitial sites in the unit cell of C-Gd_2O_3. Gd_2O_3 has p-type characteristics in the high oxygen partial pressure region[2]. Tare and Schmalzried[3] reported through an emf study that Gd_2O_3 is essentially an ionic semiconductor under oxygen partial pressures of between 10^{-2} and 10^{-1} atm. An activation energy of 1.57 eV was observed by Subbarao *et al.*[4]. Gd_2O_3 is capable of dissolving considerable amounts of tetravalent and higher valence cations and apparently produces interstitial O^{2-} ions which are mobile[5]. Diness and Roy[6] reported that a Gd_2O_3-ThO_2 solid solution having the cubic C-type structure was easily formed at a low sintering temperature, 800 °C.

The additions of lower valence cations such as Y_2O_3 to ThO_2[7], Gd_2O_3 to ThO_2[8] and Y_2O_3 to ZrO_2[9] have been reported to produce mobile O^{2-} ions due to their interstitial sites in the cubic C-type structure. The aim of this work is to characterize the influence of the ThO_2 dopant on the electrical behavior of X ThO_2+(1-X) Gd_2O_3 solid solutions. These solid solutions were chosen because Gd_2O_3 has a high activation energy for electrical conduction, ThO_2 is easily soluble up to 16 mol% in Gd_2O_3 at low temperature, 800 °C, and both oxides have good thermal stability and stoichiometric composition[6].

Experimental

Sample Preparation. C-Gd_2O_3(5N) and ThO_2(5N) polycrystallines obtained from the Rare Metallic Company were used as the starting powders. Specimens with grain size <1 μm were prepared by ultrasonic treatment. The mixed oxide was calcined at 680 °C for 10 h in air. The powder mixture was stirred for 12 h in ethyl alcohol, and then dried. The dried powder was hydrostatically pressed at 1×10^9 Pa into a pellet, presintered at 880 °C for 96 h, and then slowly cooled to room temperature. The surfaces of the presintered pellets were etched by $(NH_4)_2S_2O_8$ and H_3PO_4 solutions, respectively. The phases of the presintered pellets were investigated by X-ray diffraction technique. The X-ray patterns showed that all pellets formed cubic C-type solid solutions. The presintered specimens were reground in an agate mortar, stirred in ethyl alcohol for 24 h, and then dried. The powders were re-pelletized, resintered at 1330 °C for 40 h, and annealed at 1130 °C for 30 h to reduce the grain boundary effect. X-ray analysis results for these resintered specimens are listed in Table 1. As shown in Table 1, the specimens are all cubic C-type solid solutions.

Analysis. DTA and TGA measurements were carried

Table 1. X-ray Diffraction Results for X ThO_2+(1-X) Gd_2O_3 Solid Solutions

X	2θ	d_{obs}	h	k	l	d_{cal}	I/I_{222}
0.08	28.6034	3.1195	2	2	2	3.1233	100
	33.1415	2.7017	4	0	0	2.7049	38
	47.5749	1.9105	4	4	0	1.9127	44
	56.4518	1.6294	6	2	2	1.6311	32
0.10	28.6038	3.1194	2	2	2	3.1230	100
	33.1457	2.7012	4	0	0	2.7046	34
	47.5751	1.9104	4	4	0	1.9124	42
	56.4520	1.5933	6	2	2	1.5951	28
0.12	28.6036	3.1187	2	2	2	3.1194	100
	33.1448	2.7009	4	0	0	2.7015	37
	47.5745	1.9100	4	4	0	1.9102	44
	56.4525	1.6289	6	2	2	1.6290	34

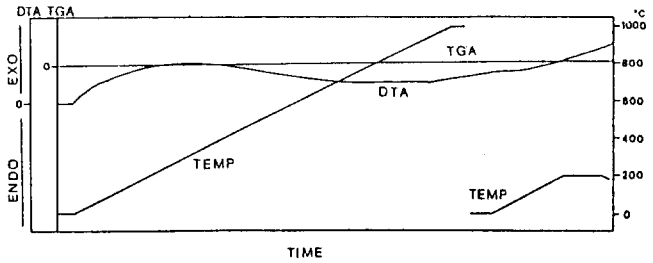

Figure 1. DTA and TGA curves of X ThO_2+(1-X) Gd_2O_3 solid solutions.

out to investigate possible phase transitions and nonstoichiometric composition. No phase transition or weight loss was observed in the Po_2 and temperature regions investigated (Figure 1).

The impurities which were analyzed by ICP are listed in Table 2 and pycnometric densities are also listed in Table 3 including lattice parameters.

Conductivity Measurements. Only the samples which had a theoretical density higher than 90% were used for dc electrical conductivity measurements to minimize grain boundary effects. Valdes' technique[10], which had been briefly described previously[11,12], was used. This technique has also been employed to measure the electrical conductivity of other oxide semiconductors[13-26], ion-doped polymers[27,28], and polymer composites[29-31]. The electrical conductivity was also determined from ac measurement as a function of frequency under atmospheric air pressure, since the data obtained by dc measurement may not represent the true lattice transport. This ac technique has been described elsewhere[32]. An oscillator, an admittance bridge and a differential amplifier as null detector were employed. Porous Pt contacts were applied to the specimen discs (1.2 cm in diameter and 0.13 cm thick) by sputtering Pt from dc plasma to weights of 1-3 mg cm^{-3}. The ac electrical behavior was analyzed with aid of an impedance plot and equivalent circuit.

Results and Discussion

The lattice parameters which have been obtained by Nelson-Riley plot (Figure 2)[33] are listed in Table 3. The lattice

Table 2. Impurity Analysis of X ThO_2+(1-X) Gd_2O_3 Solid Solutions in ppm of Impurity

Impurity \ X value	0.08	0.10	0.12
Al	7	3	5
Ca	7	7	7
Y	5	4	8
Mn	<0.1	<0.1	<0.1
Zr	8	8	10
Co	<1	2	<1
La	10	13	12
Cr	<1	1	
Cu	2	1	3
Fe	<0.1	<0.1	<0.1
V	0.5	1	2
Mg	1	3	1
Ti	1	1	0.7
Ni	2	4	1
Sr	<0.1	<0.1	1
Ce	13	16	15

Table 3. Pycnometric Densities and Lattice Parameters (LP) of X ThO_2+(1-X) Gd_2O_3 solid Solutions

X	d_{obs}(g/cm^3)	d_{cal}(g/cm^3)	d_{obs}/d_{cal}	LP(Å)
0.08	7.06	7.61	0.93	10.8133
0.10	7.11	7.65	0.93	10.8134
0.12	7.21	7.71	0.94	10.8135

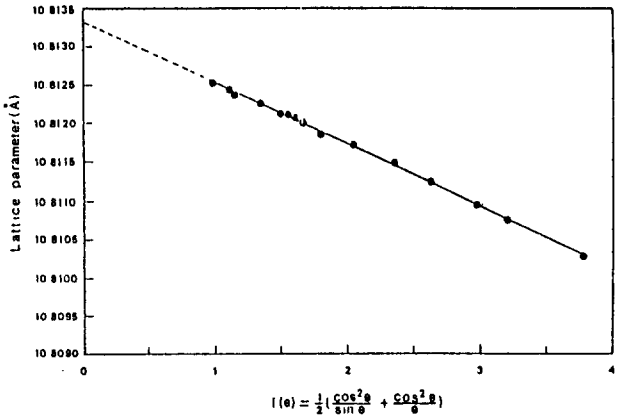

Figure 2. Lattice parameter *vs.* $f(\theta)$ for the Gd_2O_3-10 mol % ThO_2 system.

parameter *vs.* ThO_2 mol % is plotted in Figure 3 which shows that the lattice parameter of Gd_2O_3 is nearly unchanged with increasing ThO_2 mol %. This implies that X ThO_2+(1-X) Gd_2O_3 specimens are all solid solutions. The constant lattice parameters can be explained in terms of the cation size effect; the radius of the 6-coordinated T_h^{4+} (108 pm) ion is the same as that of the 6-coordinated Gd^{3+} (107.8 pm) ion[34].

Figure 4 shows the temperature dependence of the electrical conductivity. As shown in Figure 4, the conduction takes place *via* a single mechanism, since no inflection point appears, and the slopes for the 10 and 12 mol % ThO_2

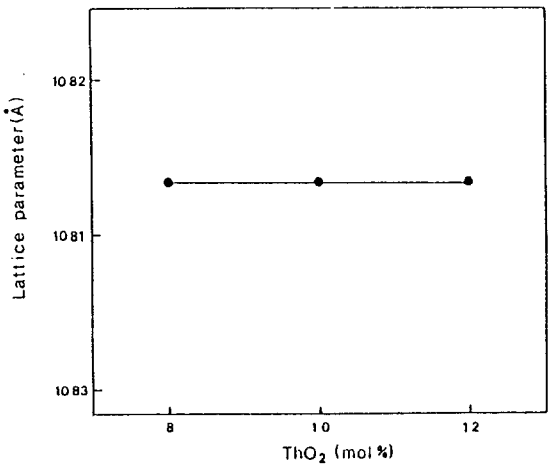

Figure 3. Lattice parameter *vs.* ThO_2 mol% for the X ThO_2+(1-X) Gd_2O_3 solid solutions.

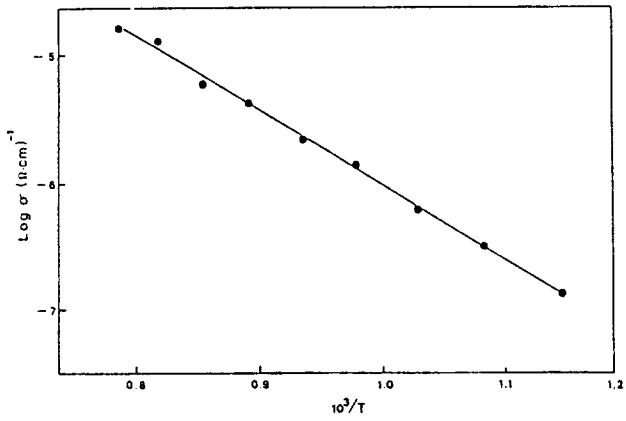

Figure 4. A typical plot of log conductivity *vs.* $10^3/T$ for the 8 mol% ThO_2-Gd_2O_3 solid solution.

Table 4. Activation Energy of Various ThO_2-Gd_2O_3 Solid Solutions

Composition of ThO_2	Po_2(atm)	Activation energy (eV)
	2×10^{-1}	1.24
8 mol%	1×10^{-3}	1.23
	1×10^{-6}	1.24
	2×10^{-1}	1.24
10 mol%	1×10^{-3}	1.21
	1×10^{-6}	1.24
	2×10^{-1}	1.25
12 mol%	1×10^{-3}	1.23
	1×10^{-6}	1.23

samples are nearly the same as that of the 8 mol % sample shown. However, the activation energy (Table 4) is smaller than that of pure Gd_2O_3[35].

The observed oxygen partical pressure (Po_2) dependencies of the electrical conductivity are shown in Figure 5. As shown in Figure 5, the electrical conductivity of the solid solution is independent of the oxygen partial pressure. Figure 6 shows a typical plot of the ac impedance data. Analysis of the complex impedance plots followed the works of Bauerle[36]

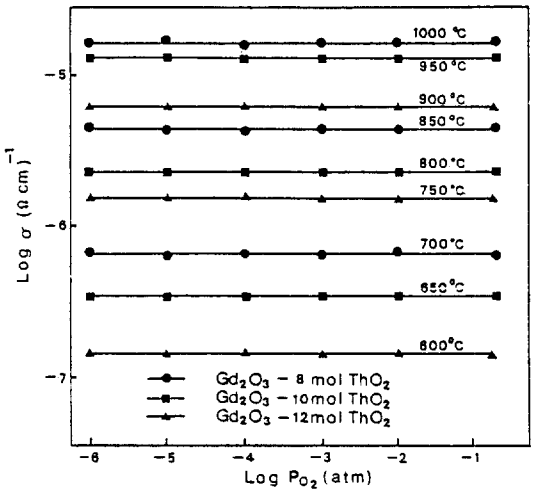

Figure 5. Log conductivity *vs.* log Po_2 for 8 mol% ThO_2, 10 mol% ThO_2 and 12 mol% ThO_2 in X ThO_2+(1-X) Gd_2O_3 solid solutions at various temperatures.

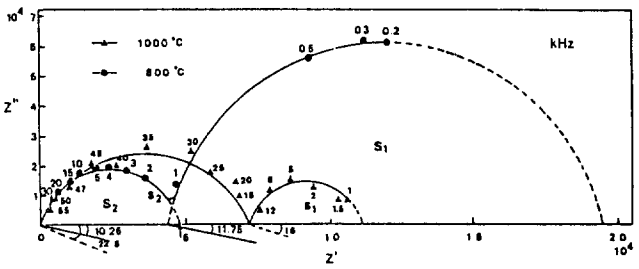

Figure 6. Impedance diagram for 8 mol% ThO_2-Gd_2O_3 solid solution at 800 and 1000 °C, 1 atm, with its 4-terminal dc conductivity marked on the Z'-axis (↑).

and was carried out in terms of the equivalent circu... In the entire experimental temperature region the intersection of S_2 with the real axis of Figure 6 agrees very well with dc conductivity. This agreement implies that the observed dc conductivity is bulk in nature.

The activation energy obtained from the temperature dependence of the intersection of S_2 agrees well with that obtained from dc measurements. The activation energy obtained from the temperature dependence of the intersection of S_1 is 2.26 eV. Bauerle[36] reported that the temperature dependence of the electrode resistance in a porous Pt electrode corresponded to a thermally activated process with a rather high activation energ., approximately 2.0-2.5 eV. The present activation energy means that the semicircle is due to the electrode reaction. The oxygen-pressure-independent bulk conduction of the system is verified by this result, and the main charge carrier is the oxygen ion.

Barret and Barry[37] found that the interstitial oxygen ions and holes are quite mobile. The diffusion process is thus most probably a migration of oxygen ions along interstitial pathways more or less associated with holes. In the present solid solutions, the interstitial oxygen ions can be formed by the dopant: $ThO_2 \rightleftharpoons 1/2\ O_i'' + 3/2\ O_2 + Th_{\dot{G}d}$, whre O_i'' is an interstitial oxygen and $Th_{\dot{G}d}$ is Th substituted on a Gd site. Doping by Th prohibits the intrinsic disorder reaction of pure Gd_2O_3: $1/2\ O_2 \rightleftharpoons 2\ \dot{h} + O_i''$ where $\dot{h}$ is an electron hole produced in the valence band. Since O_i'' ions are produced by the

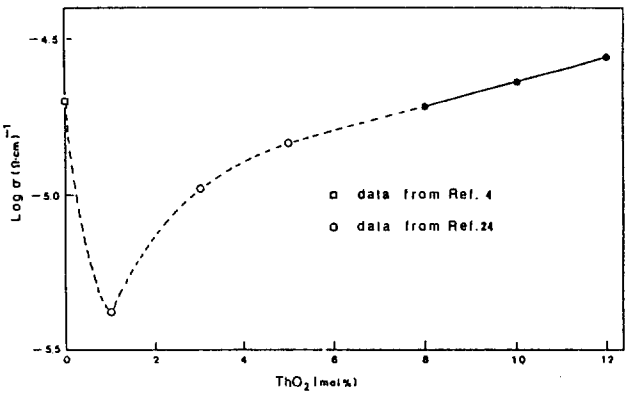

Figure 7. Log conductivity *vs.* ThO_2 mol % at 1000 °C.

Th dopant, the electron hole concentration is reduced.

The result that the conductivity is independent of oxygen pressure (Figure 5) implies that the predominant defect in X ThO_2+(1-X) Gd_2O_3 solid solutions is an oxygen interstitial and the present solid solutions are oxygen interstitial conductors. The experimental results in Figure 7 show that the conductivity increases with increasing ThO_2 mol %. This implies that the conductivity of the present solid solutions is proportional to the O_i'' concentration, $\sigma = e[O_i''](\alpha\, a\, v^2/kT)\exp[-E_m/kT]$, where e is the effective charge, α a geometrical factor, a the lattice parameter, v the frequency and E_m the activation energy for motion. As shown in Table 4, the solid solutions show a constant activation energy, regardless of the doping level. This constant activation energy is due to the nearly invariant geometry factor and lattice constant (Figure 3), and the fact that there is no change in conductivity with applied measuring frequency, as the structure does not change. From the constant activation energy, it is possible to suggest that defect clusters do not form in the present solid solutions and the defect pair is easily dissociated.

Acknowledgement. The authors are grateful to the Ministry of Education, Republic of Korea, for financial support and to professors Robert G. Sauer and Ki Hyun Yoon for helpful discussion.

References

1. Queytoux, F., Harari, A, and Collongue, R., *Bull. Soc. Fr. Ceram.*, **72**, 37 (1962).
2. Wilbert, Y., Breuil, H. and Dherbomez, N., *C.R., Hebd. Seanc. Acad. Sci. Paris*, **280**, 373 (1975).
3. Tare, V. B. and Schmalzried, H., *Z. Phys. Chem. N. F.*, **43**, 30 (1964).
4. Subbarao, G. V., Ramdas, S., Mehrotra, P. N. and Rao, C. N. R., *J. Sol. State. Chem.*, **2**, 377 (1970).
5. Berard, M. F. and Wilder, D. R., *J. Appl. Phys.*, **34**, 2818 (1963).
6. Diness, A. M. and Roy, R., *J. Mater. Sci.*, **4**, 613 (1969).
7. Subbarao, E. C., Sutter, P. H. and Hrizo, J., *J. Am. Ceram. Soc.*, **48**, 443 (1965).
8. Sibidue, F. and Hoex, M., *J. Nucl. Mater.*, **56**, 229 (1975).
9. Duwez, P., Brown, F. H. and Odell, F., *J. Electrochem. Soc.*, **98**, 356 (1951).
10. Valdes, L. B., *Proc. IRE*, **42**, 420 (1954).
11. Choi, J. S., Lee, H. Y. and Kim, K. H., *J. Phys. Chem.*, **77**, 2430 (1973).
12. Choi, J. S., Kang, Y. H. and Kim, K. H., *J. Phys. Chem.*, **81**, 2208 (1977).
13. Kim, K. H., Won, H. J. and Choi, J. S., *J. Phys. Chem. Solids*, **45**, 1259 (1984).
14. Kim, K. H., Oh, E. J. and Choi, J. S., *J. Phys. Chem. Solids*, **45**, 1265 (1984).
15. Kim, K. H., Lee, S. H. and Choi, J. S., *J. Phys. Chem. Solids*, **46**, 331 (1985).
16. Kim, K. H., Lee, S. H., Kim, Y. R. and Choi, J. S., *Bull. Kor. Chem. Soc.*, **6**, 11 (1985).
17. Kim, K. H., Yoon, K. H. and Choi, J. S., *J. Phys. Chem. Solids*, **46**, 1061 (1985).
18. Kim, K. H., Jun, J. H. and Choi, J. S., *J. Phys. Chem. Solids*, **46**, 1173 (1985).
19. Kim, K. H., Choi, J. S. and Chung, W. Y., *J. Phys. Chem. Solids*, **47**, 117 (1986).
20. Kim, K. H., Lee, S. H. and Choi, J. S., *Bull. Kor. Chem. Soc.*, **7**, 341 (1986).
21. Kim, K. H., Oh, E. J. and Choi, J. S., *J. Phys. Chem. Solids*, **47**, 833 (1986).
22. Kim, K. H., Won, H. J. and Choi, J. S., *J. Phys. Chem. Solids*, **48**, 383 (1987).
23. Kim, K. H., Yim, D. Y., Park, S. H. and Choi, J. S., *J. Phys. Chem. Solids*, **49**, 151 (1988).
24. Kim, K. H., Park, S. H., Choi, J. S. and Hyung, K. W., *J. Phys. Chem. Solids*, **49**, 1019 (1988).
25. Choi, K. M., Kim, K. H. and Choi, J. S., *J. Phys. Chem. Solids*, **49**, 1027 (1988).
26. Lee, D. Y., Kim, D., Kim, K. H. and Choi, J. S., *Bull. Kor. Chem. Soc.*, **9**, 333 (1988).
27. Choi, K. M., Kim, K. H. and Choi, J. S., *J. Phys. Chem. Solids*, **50**, 283 (1989).
28. Choi, K. M., Kim, K. H. and Choi, J. S., *J. Phys. Chem.*, **93**, 4659 (1989).
29. Kim, K. H., Lee, S. H. and Choi, J. S., *J. Appl. Polym. Sci.*, **34**, 2537 (1987).
30. Kim, K. H., Lee, S. H., Heo, G. and Choi, J. S., *J. Phys. Chem. Solids*, **48**, 895 (1987).
31. Jun, J. H., Lee, S. H., Kim, K. H. and Choi, J. S., *J. Phys. Chem. Solids, in press (1989).*
32. Hohnke, D. K., *J. Phys. Chem. Solids*, **41**, 777 (1980).
33. Nelson, J. B. and Riley, D. P., *Proc. Phys. Soc.*, **57**, 160 (1945).
34. Huheey, J. E. "Inorganic Chemistry" (Edited by Huheey, J. E.), p. 73, Harper & Row, New York (1978).
35. Subbarao, G. V., Ramdas, S., Mehrotra, P. N. and Rao, C. N. R., *J. Sol. State Chem.*, **2**, 377 (1970).
36. Bauerle, J. E., *J. Phys. Chem. Solids*, **30**, 2651 (1969).
37. Barret, M. F. and Barry, T. I., *J. Inorg. Nucl. Chem.*, **27**(7), 1483 (1965).